Semiclassical description of nonadiabatic quantum dynamics: Application to the S_1-S_2 conical intersection in pyrazine

Michael Thoss and William H. Miller[a)]
Department of Chemistry, University of California, and Chemical Sciences Division, Lawrence Berkeley National Laboratory, Berkeley, California 94720

Gerhard Stock
Faculty of Physics, University Freiburg, D-79104 Freiburg, Germany

(Received 26 January 2000; accepted 24 March 2000)

A recently proposed semiclassical approach to the description of nonadiabatic quantum dynamics [G. Stock and M. Thoss, Phys. Rev. Lett. **78**, 578 (1997), X. Sun and W. H. Miller, J. Chem. Phys. **106**, 916 (1997)] is applied to the S_1-S_2 conical intersection in pyrazine. This semiclassical method is based on a transformation of discrete quantum variables to continuous variables, thereby bypassing the problem of a classical treatment of discrete quantum degrees of freedom such as electronic states. Extending previous work on small systems, we investigate the applicability of the semiclassical method to larger systems with strong vibronic coupling. To this end, we present results for several pyrazine models of increasing dimensionality and complexity. In particular, we discuss the quality and performance of the semiclassical approach when the number of nuclear degrees of freedom is increased. Comparison with quantum-mechanical calculations and experimental results shows that the semiclassical method is able to describe the ultrafast dynamics in this system. [S0021-9606(00)01323-4]

I. INTRODUCTION

The photophysics and photochemistry of excited electronic states in polyatomic molecules represents a field of continuing interest in chemical physics. Recent experimental and theoretical investigations have revealed that for the photoinduced dynamics of polyatomic molecules transitions between different Born–Oppenheimer (adiabatic) potential-energy surfaces (PES) are the rule rather than the exception.[1–4] A variety of interesting processes is described by nonadiabatic dynamics, for example, radiationless transitions (internal-conversion and intersystem-crossing processes), electron-transfer processes, and photoinduced isomerization reactions.

A realistic theoretical description of these processes typically involves the treatment of two or more electronic states and several or (for larger molecules) many vibrational modes with strong electronic–vibrational interactions. Therefore, the applicability of exact quantum-mechanical basis-set methods is, in general, limited to smaller molecules or models with reduced dimensionality. In recent years, there has been significant progress in the development of quantum-mechanical approaches for describing nonadiabatic dynamics in larger molecules or in the condensed phase, including time-dependent self-consistent field (TDSCF) schemes,[5–8] multiconfigurational extensions of the TDSCF approximation such as the multiconfiguration time-dependent Hartree (MCTDH) method,[9–11] path-integral formulations,[12–18] and the reduced-density matrix approach.[19–25] Besides these fully quantum-mechanical approaches, numerous methods based on classical or semiclassical concepts have been developed. In particular for larger systems, classical methods are an interesting alternative, because they are expected to overcome some of the limitations of fully quantum mechanical approaches such as, for example, the exponential scaling of the computational effort with the number of degrees of freedom (DoF) in basis-set methods or the restriction to quadratic potentials for the bath DoF in influence-functional-based path-integral methods.

A classical description is straightforward in cases where both the system under consideration and the observable to be calculated have an obvious classical analog. It is less clear, however, how to incorporate discrete quantum-mechanical DoF which do not possess an obvious classical counterpart (such as the electronic states in nonadiabatic dynamics) into a classical theory.

A natural strategy is to describe the nuclear dynamics by classical mechanics while still retaining a quantum description for the discrete (electronic) DoF. There are several ways this mixed quantum-classical methodology has been implemented,[26–44] most notably the classical-path approach (or Ehrenfest model)[26–32] and the surface-hopping method.[33–39] Both methods have been applied successfully to a variety of situations; however, due to the approximations employed in these models, there are well-known shortcomings in both approaches, e.g., classical-path methods do not obey microreversibility and the hopping processes of the surface-hopping methods destroy the coherence of the quantum system.[45]

A more rigorous and dynamically consistent formulation of the coupling of quantum and classical DoF can be obtained within the path-integral formalism. Employing a

[a)]Electronic mail: miller@neon.cchem.berkeley.edu

stationary-phase evaluation of the path integral, Pechukas showed that the classical particles move in a nonlocal force field generated by the quantum particles, thus reflecting the nonlocal nature of the quantum system.[46] Pechukas' theory is conceptionally illuminating and is ''semiclassically exact'' in the sense that it requires only the basic semiclassical Van-Vleck–Gutzwiller approximation[47] to the quantum propagator; the calculation of nonlocal forces, however, is in practice more cumbersome than the exact quantum calculation.[48]

A very different approach to the problem of nonadiabatic quantum dynamics was taken by McCurdy, Meyer, and Miller[49–52] some years ago. Employing various quantum-classical analogies, they replaced the electronic states by classical DoF, thereby yielding a classical Hamiltonian in terms of the nuclear coordinates and momenta, and coordinates and momenta for the electronic DoF. Within this ansatz, classical trajectories could thus be computed for the full vibronic system, thereby treating electronic and nuclear DoF on an equal footing. Most of the early applications of these models utilized the ''quasiclassical'' approximation[53] for treating initial and final conditions of the trajectories; in the ''classical electron-analog'' model of Meyer and Miller,[51] for example, the equations of motion for the vibronic system are the same as in the classical-path (Ehrenfest) approach, but the way the boundary conditions are applied makes the models quite different. Meyer and Miller also discussed the semiclassical version of their model (within the framework of ''classical *S*-matrix'' theory[54]) and showed that for simple two-state curve crossing problems it was a considerable improvement over the quasiclassical version.

More recently, Stock and Thoss[55,56] have used a quantum-mechanical bosonization technique[57] to map the discrete (electronic) DoF onto continuous DoF (harmonic oscillators). This formulation is quantum-mechanically exact and has a well-defined semiclassical limit, since both electronic and nuclear DoF are described by continuous variables. Furthermore, the formalism allows us to make contact with the spin-coherent-state representation[58] of the semiclassical propagator. The classical limit of the mapping approach yields the same Hamiltonian as the Meyer–Miller model, so the two formulations are equivalent at the semiclassical level. Other aspects of the mapping approach and its relation to the Meyer–Miller model are discussed in Refs. 56, 59 and 60.

This new semiclassical approach has been applied to several small systems including nonadiabatic bound-state dynamics of several spin-boson type models with up to three vibrational modes,[55,56] a series of scattering-type test problems suggested by Tully,[59] a model for laser driven population transfer between two adiabatic PES,[61] and the photodissociation dynamics of ozone[62] and ICN.[63] The results of these numerical studies are quite promising. The main purpose of the present paper is to study the performance of this semiclassical method for larger systems. To this end, we have chosen the nonadiabatic dynamics of the pyrazine molecule after photoexcitation to the S_2 state as a test example.

The nonadiabatic dynamics induced by the conical intersection of the $S_1(\mathrm{n},\pi^*)$ and the $S_2(\pi,\pi^*)$ PES of pyrazine is one of the most extensively studied examples of vibronic coupling in a polyatomic molecule. During the last decade, there have been several theoretical investigations of this system. The methods used include reduced dimensionality quantum basis-set calculations (including the three or four most important vibrational modes),[64–70] a path-integral treatment modeling the remaining 20 vibrational modes as a weakly coupled bath,[17,18] and various classical methods.[32,71–73] Very recently, a quantum calculation in full dimensionality using the MCTDH method has been performed.[74–76] Therefore, this system is well-suited as a test of the semiclassical method.

The outline of the paper is as follows. In Sec. II we introduce the model Hamiltonian to describe the nonadiabatic dynamics, define the observables of interest, and briefly review the theory of the semiclassical approach. Section III presents the results of numerical calculations for several pyrazine models of increasing dimensionality and complexity: a four-mode model including the four most strongly coupled normal modes, a system-bath model, which is obtained by coupling the four-mode model to an increasing number of bath modes, and, finally, a realistic 24-mode model. Based on comparison with quantum-mechanical results, which have been obtained by Meyer, Cederbaum, and co-workers,[74–76] we discuss the performance of the semiclassical approach for the different models. Section IV summarizes and concludes.

II. THEORY

A. Model Hamiltonian and observables of interest

Let us consider a general vibronic coupling problem. As is well known, a vibronic coupling problem can be described in the adiabatic or in the diabatic electronic representation.[1,4] Adopting a diabatic electronic basis $\{|\phi_1\rangle,\ldots,|\phi_M\rangle\}$, the molecular Hamiltonian comprising M coupled electronic states and N vibrational DoF can be written in the form

$$\mathcal{H}=T(\mathbf{p})+V_0(\mathbf{x})+\sum_{n,m}|\phi_n\rangle V_{nm}(\mathbf{x})\langle\phi_m|, \tag{2.1}$$

where $T(\mathbf{p})$ denotes the kinetic energy of the nuclei, V_{nm} represents the elements of the diabatic potential matrix, and V_0 is a state-independent potential term.

The semiclassical approach to be outlined in the next section is independent of the specific form of the potential V_0 and the diabatic potential matrix V_{nm}. In order to introduce some notation and to facilitate the following discussion, however, it is convenient to specify the Hamiltonian in the model form which is used later. In the applications considered in this paper, the state-independent part of the Hamiltonian is given by the harmonic approximation for the potential energy in the electronic ground state

$$T(\mathbf{p})+V_0(\mathbf{x})=\sum_{j=1}^{N}\frac{\omega_j}{2}(p_j^2+x_j^2), \tag{2.2}$$

where ω_j is the vibrational frequency and x_j and p_j are, respectively, the dimensionless position and momentum operators of the jth vibrational mode. (We use units with $\hbar=1$ throughout the paper.) As is common practice in vibronic

coupling theory,[1,4] the diabatic potential matrix V_{nm} is approximated by a Taylor expansion around the equilibrium geometry of the electronic ground state

$$V_{nn}=E_n+\sum_j \kappa_j^{(n)}x_j+\sum_{i,j}\kappa_{i,j}^{(n)}x_ix_j, \tag{2.3a}$$

$$V_{nm}=V_{nm}(\mathbf{0})+\sum_j \lambda_j^{(nm)}x_j+\sum_{i,j}\lambda_{i,j}^{(nm)}x_ix_j, \quad n\neq m. \tag{2.3b}$$

Here, $E_n=V_{nn}(\mathbf{0})$ denotes the vertical excitation energy of state $|\phi_n\rangle$, the $\kappa_j^{(n)}$ are the gradients of the excited-state potential energy function at the equilibrium geometry of the ground state, and the $\kappa_{i,j}^{(n)}$ account for the changes in vibrational frequencies and rotation of the normal coordinates in the excited states (the so-called Dushinsky effect[77]). The expansion of the interstate-coupling matrix elements in Eq. (2.3b) is determined by the vibronic coupling constants $\lambda_j^{(nm)}$ and $\lambda_{i,j}^{(nm)}$. The Taylor expansion (2.3) has been shown to be a good approximation for observables which are based on short-time dynamics in the Franck–Condon zone such as absorption or resonance Raman spectra (see, for example, Ref. 4 and references therein).

In this work we are interested in the nonadiabatic dynamics of the pyrazine molecule after photoexcitation to the S_2 electronic state. In particular, we will present results for the absorption spectrum in this energy region which can be obtained from the Fourier transform of the autocorrelation function

$$J(t)=\langle\Psi_i|e^{-i\mathcal{H}t}|\Psi_i\rangle, \tag{2.4}$$

using the well-known relation

$$I(\omega)\propto\omega\,\mathrm{Re}\int_0^\infty \mathrm{d}t\, e^{i(\omega+\varepsilon_0)t}J(t). \tag{2.5}$$

Here, the initial state $|\Psi_i\rangle$ is (within the Condon approximation for the transition dipole moment and for low temperature[78]) given by a product of the vibrational ground state of the molecule and the second excited electronic state

$$|\Psi_i\rangle=|\phi_2\rangle|\mathbf{v}_i=\mathbf{0}\rangle, \tag{2.6}$$

and ε_0 denotes the energy of the vibronic ground state of the molecule.

B. Semiclassical description

A semiclassical description is well established when both the Hamilton operator of the system and the quantity to be calculated have a well-defined classical analog. For example, there exist several semiclassical methods for calculating the vibrational autocorrelation function on a single excited electronic surface (which is related to the Franck–Condon spectrum).[79–84] In particular, semiclassical methods based on the initial-value representation (IVR)[85] (which circumvent the cumbersome root-search problem in boundary-value-based semiclassical methods) have been successfully applied to a variety of systems (see, for example, the reviews[86–88] and references therein). These methods cannot be applied directly to nonadiabatic dynamics, because the Hamilton operator for the vibronic coupling problem [Eq. (2.1)] involves discrete DoF (discrete electronic states) which do not possess an obvious classical counterpart.

Recently, Stock and Thoss[55,56] and Sun and Miller[59] have proposed a new approach which extends the applicability of well-established semiclassical methods to systems with discrete DoF. The key idea in this approach is to represent the discrete (electronic) DoF by continuous harmonic-oscillator DoF which possess a well-defined classical analog. This transformation can be accomplished in different ways: Sun and Miller's formulation is based on a requantization of the classical electron-analog model of Meyer and Miller.[51] Stock and Thoss have used a generalization of Schwinger's theory of angular momentum[57] to map a discrete M-level system onto M harmonic oscillators via the following relations for the operators and the basis states:

$$|\phi_n\rangle\langle\phi_m|\rightarrow a_n^\dagger a_m, \tag{2.7a}$$

$$|\phi_n\rangle\rightarrow|0_1,\ldots,1_n,\ldots,0_M\rangle. \tag{2.7b}$$

Here a_n and $a_m^\dagger$ are the usual oscillator creation and annihilation operators with bosonic commutation relations $[a_n,a_m^\dagger]=\delta_{nm}$ and $|0_1,\ldots,1_n,\ldots,0_M\rangle$ denotes a harmonic-oscillator eigenstate with a single quantum excitation in the mode n. Introducing, furthermore, Cartesian electronic variables

$$X_n=(a_n^\dagger+a_n)/\sqrt{2}, \tag{2.8a}$$

$$P_n=i(a_n^\dagger-a_n)/\sqrt{2}, \tag{2.8b}$$

the molecular Hamiltonian in the continuous representation reads

$$H=h_0(\mathbf{x},\mathbf{p})+\frac{1}{2}\sum_{n,m}(X_nX_m+P_nP_m)V_{nm}(\mathbf{x}), \tag{2.9a}$$

$$h_0(\mathbf{x},\mathbf{p})=T(\mathbf{p})+V_0(\mathbf{x})-\frac{1}{2}\sum_n V_{nn}(\mathbf{x}). \tag{2.9b}$$

As has been discussed in detail in Ref. 56, the Hamilton operator (2.9) is equivalent to the Hamiltonian (2.1) within the physical subspace (which is the image of the M-level Hilbert space under the mapping (2.7b), i.e., the subspace of the M-oscillator Hilbert space with a single quantum excitation). In particular, we have the following identity for the autocorrelation function:

$$\begin{aligned}J(t)&=\langle\phi_i|\langle\mathbf{v}_i|e^{-i\mathcal{H}t}|\mathbf{v}_i\rangle|\phi_i\rangle\\&=\langle 0_1,\ldots,1_i,\ldots,0_M|\langle\mathbf{v}_i|e^{-iHt}|\mathbf{v}_i\rangle\\&\quad\times|0_1,\ldots,1_i,\ldots,0_M\rangle.\end{aligned} \tag{2.10}$$

In contrast to $\mathcal{H}$, the Hamiltonian H has a well-defined classical analog and therefore any of the well-established semiclassical approximations for the quantum propagator e^{-iHt} can be used to obtain a semiclassical approximation for the autocorrelation function. In this paper, we use the Herman–Kluk (coherent-state) IVR of the semiclassical

propagator,[80] which for a general n-dimensional system can be written as

$$e^{-iHt}=\int \frac{d\mathbf{q}_0\, d\mathbf{p}_0}{(2\pi)^n}|\mathbf{q}_t\mathbf{p}_t\rangle C_t e^{iS_t}\langle \mathbf{q}_0\mathbf{p}_0|, \tag{2.11}$$

where $(\mathbf{p}_0,\mathbf{q}_0)$ are initial momenta and coordinates for classical trajectories, $\mathbf{p}_t=\mathbf{p}_t(\mathbf{p}_0,\mathbf{q}_0)$ and $\mathbf{q}_t=\mathbf{q}_t(\mathbf{p}_0,\mathbf{q}_0)$ are the classically time-evolved phase space variables and S_t is the classical action integral along the trajectory. The pre-exponential factor C_t is given by

$$C_t(\mathbf{p_0},\mathbf{q_0})=\sqrt{\det\left[\frac{1}{2}\left(\gamma^{1/2}\frac{\partial \mathbf{q}_t}{\partial \mathbf{q}_0}\gamma^{-1/2}+\gamma^{-1/2}\frac{\partial \mathbf{p}_t}{\partial \mathbf{p}_0}\gamma^{1/2}-i\gamma^{1/2}\frac{\partial \mathbf{q}_t}{\partial \mathbf{p}_0}\gamma^{1/2}+i\gamma^{-1/2}\frac{\partial \mathbf{p}_t}{\partial \mathbf{q}_0}\gamma^{-1/2}\right)\right]}. \tag{2.12}$$

It involves a combination of the elements of the monodromy matrix

$$\mathbf{M}_t=\begin{pmatrix}\frac{\partial \mathbf{p}_t}{\partial \mathbf{p}_0} & \frac{\partial \mathbf{p}_t}{\partial \mathbf{q}_0}\\ \frac{\partial \mathbf{q}_t}{\partial \mathbf{p}_0} & \frac{\partial \mathbf{q}_t}{\partial \mathbf{q}_0}\end{pmatrix}. \tag{2.13}$$

In the above expression, γ denotes an n-dimensional diagonal matrix, with the element γ_j being the width parameter for the coherent state of the jth dimension. The coordinate space representation of an n-dimensional coherent state is the product of n one-dimensional minimum uncertainty wave packets

$$\langle \mathbf{x}|\mathbf{pq}\rangle=\prod_{j=1}^{n}\left(\frac{\gamma_j}{\pi}\right)^{1/4}e^{-\gamma_j/2(x_j-q_j)^2+ip_j(x_j-q_j)}. \tag{2.14}$$

Within the applicability of the semiclassical approximation, the propagator (2.11) is rather insensitive to the particular value of the width parameters γ_j, but this parameter can of course affect the numerical efficiency of the calculation. In the numerical studies presented below, we have chosen the width γ_j as the width of the harmonic ground state of the jth vibrational mode. In the dimensionless units used in this work, this choice corresponds to $\gamma_j=1$ for all DoF. In the remainder of the paper, all coherent states have this value of the width parameter.

Inserting the Hermann–Kluk propagator (2.11) into Eq. (2.10), we obtain the semiclassical expression for the S_2 autocorrelation function of our model system

$$\begin{aligned}J(t)=\int \frac{d\mathbf{X}_0\, d\mathbf{P}_0}{(2\pi)^M}\int \frac{d\mathbf{x}_0\, d\mathbf{p}_0}{(2\pi)^N}&\langle 0|X_{1t}P_{1t}\rangle\langle 1|X_{2t}P_{2t}\rangle\\ &\times\langle \mathbf{0}|\mathbf{x}_t\mathbf{p}_t\rangle C_t e^{iS_t}\langle \mathbf{x}_0\mathbf{p}_0|\mathbf{0}\rangle\langle X_{10}P_{10}|0\rangle\langle X_{20}P_{20}|1\rangle.\end{aligned} \tag{2.15}$$

Here, $|1\rangle$ and $|0\rangle$ denote harmonic-oscillator eigenfunctions (resulting from the mapping of the electronic state $|\phi_2\rangle \rightarrow|0\rangle|1\rangle$).

The calculation of the autocorrelation function via Eq. (2.15) is a challenging task because it involves a multidimensional integral over an oscillating integrand. In addition, the pre-exponential factor C_t can become large for chaotic trajectories. Therefore, it is rather difficult to converge the integral for longer times (which for the present system means times larger then 20 fs) using simple Monte Carlo integration schemes. Several smoothing techniques have been proposed to overcome this well-known problem of semiclassical propagators.[83,89–93] In this work, we have adapted the method of Walton and Manolopoulos[83] to our system. This method combines the Herman–Kluk propagator with the cellular dynamics algorithm of Heller.[81] It is based on the Filinov[94,95] or stationary-phase Monte Carlo method.[96] The basic idea of this technique is to integrate out the local oscillations analytically using a linearization of the integrand over a small phase-space cell. Applying this method, we obtain the following expression for the autocorrelation function:

$$\begin{aligned}J(t)=\int \frac{d\mathbf{X}_0\, d\mathbf{P}_0}{(2\pi)^M}\int \frac{d\mathbf{x}_0\, d\mathbf{p}_0}{(2\pi)^N} f_t(\mathbf{X}_0,\mathbf{P}_0,\mathbf{x}_0,\mathbf{p}_0)&\langle 0|X_{1t}P_{1t}\rangle\\ &\times\langle 1|X_{2t}P_{2t}\rangle\langle \mathbf{0}|\mathbf{x}_t\mathbf{p}_t\rangle C_t e^{iS_t}\langle \mathbf{x}_0\mathbf{p}_0|\mathbf{0}\rangle\langle X_{10}P_{10}|0\rangle\\ &\times\langle X_{20}P_{20}|1\rangle.\end{aligned} \tag{2.16}$$

The only difference from Eq. (2.15) is the smoothing function f_t, which is given by[83]

$$f_t(\mathbf{X}_0,\mathbf{P}_0,\mathbf{x}_0,\mathbf{p}_0)=\frac{\alpha^{N+M}}{\sqrt{\det(\mathbf{A})}}\exp\{(1/4)\mathbf{b}^T\mathbf{A}^{-1}\mathbf{b}\}. \tag{2.17}$$

Here, the vector $\mathbf{b}$ is defined by

$$\mathbf{b}=(\mathbf{b_p},\mathbf{b_q})^T, \tag{2.18a}$$

$$\begin{aligned}\mathbf{b_p}=&\frac{1}{2}\left(\frac{\partial \mathbf{X_t}^T}{\partial \mathbf{P_0}}+i\frac{\partial \mathbf{P_t}^T}{\partial \mathbf{P_0}}\right)(\mathbf{X}_t-i\mathbf{P}_t)\\ &+\frac{1}{2}\left(\frac{\partial \mathbf{x_t}^T}{\partial \mathbf{p_0}}+i\frac{\partial \mathbf{p_t}^T}{\partial \mathbf{p_0}}\right)(\mathbf{x}_t-i\mathbf{p}_t)\\ &+\frac{1}{2}(\mathbf{P}_0-i\mathbf{X}_0)+\frac{1}{2}(\mathbf{p}_0-i\mathbf{x}_0),\end{aligned} \tag{2.18b}$$

$$\begin{aligned}\mathbf{b_q}=&\frac{1}{2}\left(\frac{\partial \mathbf{X_t}^T}{\partial \mathbf{X_0}}+i\frac{\partial \mathbf{P_t}^T}{\partial \mathbf{X_0}}\right)(\mathbf{X}_t-i\mathbf{P}_t)\\ &+\frac{1}{2}\left(\frac{\partial \mathbf{x_t}^T}{\partial \mathbf{x_0}}+i\frac{\partial \mathbf{p_t}^T}{\partial \mathbf{x_0}}\right)(\mathbf{x}_t-i\mathbf{p}_t)\\ &+\frac{1}{2}(\mathbf{X}_0+i\mathbf{P}_0)+\frac{1}{2}(\mathbf{x}_0+i\mathbf{p}_0).\end{aligned} \tag{2.18c}$$

The positive definite matrix $\mathbf{A}$ involves the monodromy matrix $\mathbf{M}_t$ [see Eq. (2.13)] and the smoothing parameter α

$$\mathbf{A}=\tfrac{1}{4}\mathbf{M}_t^T\mathbf{M}_t+\tfrac{1}{4}+\alpha. \tag{2.19}$$

The parameter α determines the size of the phase-space cell over which the integrand is smoothed. (In general, α can be a matrix.[83,95] Here, we use the same value of α for coordinates and momenta in all DoF.) For larger α, this cell size becomes smaller and in the limit $\alpha\to\infty$ the original Herman–Kluk expression (2.15) is reobtained. For finite values of α, the integrand with the smoothing function f_t is in general less oscillatory than the original integrand in Eq. (2.15) and, therefore, easier to integrate by Monte Carlo methods.

III. APPLICATION

In this section, we shall apply the semiclassical method outlined above to different vibronic-coupling models for the S_1–S_2 conical intersection in pyrazine. This system was chosen because it represents one of the most extensively studied examples of vibronic coupling in a polyatomic molecule. On the experimental side, manifestations of the strong vibronic coupling in this system have been found in absorption, fluorescence, and resonance Raman spectra.[97–103] On the theoretical side, the conical intersection between the S_1 and the S_2 electronic state has been characterized in great detail in a series of *ab initio* calculations of increasing accuracy and completeness.[4,66,67,69,76] Based on these *ab initio* calculations, the dynamics and spectroscopy of the S_1 and the S_2 state have been investigated in considerable detail.[4,64,67,70,76] It was shown that the strong vibronic coupling triggers an ultrafast $S_1\to S_2$ internal conversion process, which becomes manifest, for example, in the diffuse S_2-absorption band. Exhibiting complex electronic and vibrational dynamics, this system provides a stringent test for an approximate description.

A. Four-mode pyrazine model

First, we consider a four-mode model of the S_1–S_2 conical intersection in pyrazine, which was developed by Domcke and co-workers.[69] This model has been used as a test example for several approximate methods.[17,18,71,32,72] The model Hamiltonian has the form of Eqs. (2.1) and (2.3), where the Taylor expansion of the diabatic potential matrix is terminated after the first order

$$\mathbf{V}=\begin{pmatrix} E_1+\sum_{j\in G}\kappa_j^{(1)}x_j & \lambda x_{10a} \\ \lambda x_{10a} & E_2+\sum_{j\in G}\kappa_j^{(2)}x_j \end{pmatrix}. \tag{3.1}$$

Besides the nontotally symmetric coupling mode ν_{10a} (which, for symmetry reasons, is the only mode that can couple the two electronic states in the first order), the three most strongly coupled totally symmetric (Condon-active) modes are taken into account in this model. The set of these modes is denoted by $G=\{\nu_1,\nu_{6a},\nu_{9a}\}$. The parameters of this model Hamiltonian have been obtained by Domcke and co-workers by high-level *ab initio* calculations.[69] It has been shown that the essential features of the electronic spectra and the ultrafast radiationless decay can be understood from this model.

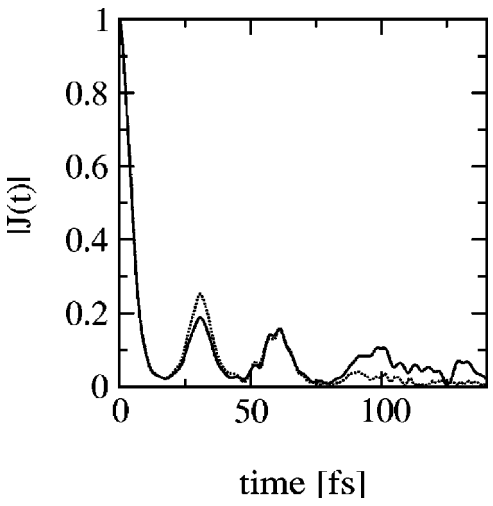

FIG. 1. Modulus of the autocorrelation function for the four-mode model. The full line is the quantum result and the dotted line is the semiclassical result.

Let us first focus on the autocorrelation function of the model system after photoexcitation to the S_2 electronic state. Figure 1 shows the modulus of the autocorrelation function up to 130 fs. The exact quantum results (full line) are compared to the semiclassical results (dotted line). As is well known from previous studies, the autocorrelation function exhibits a fast initial decay, reflecting the initial displacement of the wave packet on the S_2 surface. The suppression of the ensuing recurrences (which is absent for the uncoupled system, i.e., $\lambda=0$[64]) reflects the ultrafast electronic dephasing in the S_2 electronic state of pyrazine. This dephasing process is incomplete due to the limited density of states of the four-mode model. It is seen that the semiclassical result reproduces all essential features of the autocorrelation function up to 100 fs. Both the first two recurrences and the high frequency modulations are well described. Upon closer inspection one recognizes that the fine structure of the autocorrelation function is better reproduced than the overall damping of the amplitude, e.g., the semiclassical result underestimates the damping of the first recurrence and has too small an amplitude for times $t>80$ fs. This deviation is presumably related to the nonunitarity of the semiclassical approximation.[104]

The semiclassical result in Fig. 1 has been obtained using a smoothing parameter of $\alpha=5\cdot10^4$. The dependence of the final result, as well as the numerical effort on the value of the parameter α, is demonstrated in Fig. 2. Panel (a) shows the modulus of the autocorrelation function for three different values of the smoothing parameter ($\alpha=5\cdot10^4$, $5\cdot10^5$, $5\cdot10^6$), and panel (b) displays the corresponding statistical error of the Monte Carlo integration. In all three cases, the results are based on the propagation of 10^7 trajectories. In general, a smaller value of α results in a faster convergence of the Monte Carlo integration because the integrand is less oscillatory. On the other hand, the value of α which is required to obtain the true semiclassical result increases with

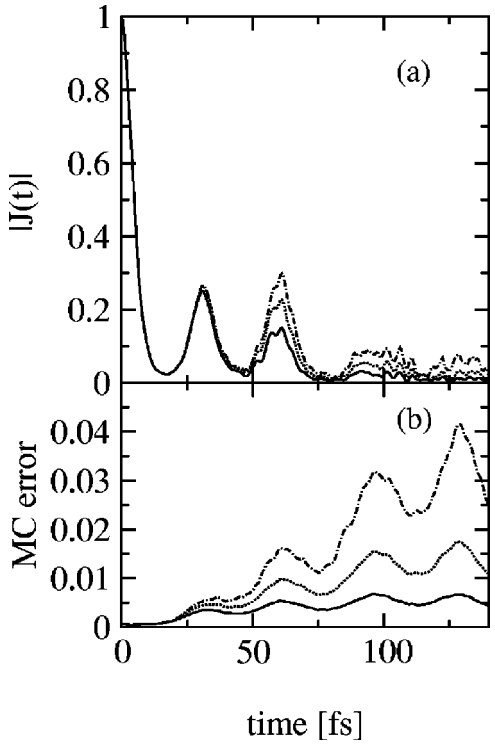

FIG. 2. Dependence of the semiclassical result on the smoothing parameter α. Panel (a) shows the modulus of the autocorrelation function for smoothing parameters $\alpha=5\cdot10^4$ (full line), $\alpha=5\cdot10^5$ (dotted line), and $\alpha=5\cdot10^6$ (dashed-dotted line). Panel (b) displays the corresponding Monte Carlo error.

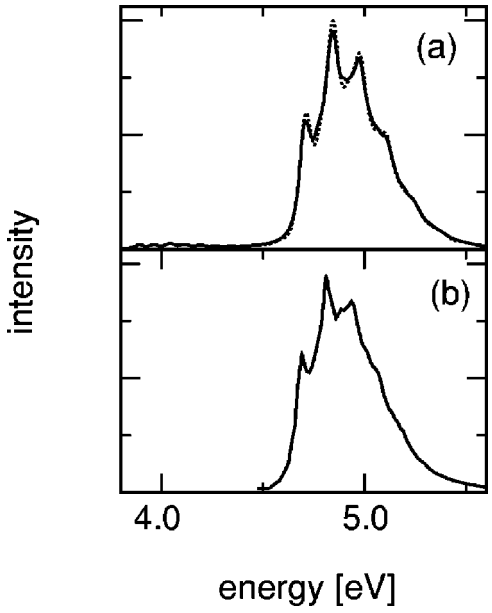

FIG. 3. Absorption spectrum of pyrazine in the energy region of the S_1–S_2 conical intersection. Shown are (a) quantum-mechanical (full line) and semiclassical (dotted line) results for the four-mode model (including a phenomenological dephasing constant of $T_2=30$ fs), and (b) the experimental data (Ref. 106).

time, because the nonlinearity of the classical dynamics develops phase-space structures on smaller and smaller scales and therefore, the size of the phase-space cell over which the linearization is valid shrinks.[83,105] Both trends are clearly visible in Fig. 2: For very short times ($t<20$ fs), the smoothing has hardly any effect on the result, because the dynamics is approximately linear. Between $t=20$ fs and $t=80$ fs, the value of α which is necessary to obtain the true semiclassical result increases from $\alpha=5\cdot10^4$ to $\alpha=5\cdot10^6$. The latter value requires many more trajectories to converge the Monte Carlo integral to the same statistical error [approximately an order of magnitude more at $t=80$, cf. Fig. 2, panel (b)]. For even longer times ($t>80$ fs) a value of $\alpha>5\cdot10^6$ is necessary to obtain the true semiclassical result, requiring a very large number of trajectories. In particular, for the larger systems discussed below, it is not feasible to use that many trajectories because the numerical effort per trajectory scales with $(N+M)^3$ (due to the calculation of the pre-exponential factor C_t). The value of $\alpha=5\cdot10^4$, which will be used in the remainder of the paper, represents a compromise between the numerical efficiency of the calculation and the aim to obtain the true semiclassical result at least for short times. The comparison of the three different results in Fig. 2 also reveals that a smaller value of the smoothing parameter leads to a stronger damping of the overall amplitude, whereas the fine structure of the autocorrelation function is nearly unaffected. Therefore, the position of the peaks in the absorption spectrum is expected to be rather insensitive to changes in the value of α, but the width of the peaks will increase with decreasing α.

The S_2 absorption spectrum is displayed in Fig. 3. Panel (a) compares the semiclassical and the quantum result and panel (b) shows the experimental data from Ref. 106. Both theoretical results have been obtained by Fourier transformation of the autocorrelation function. As has been done previously, a phenomenological dephasing constant $T_2=30$ fs has been included to reproduce the homogeneous width of the experimental spectrum [i.e., $J(t)$ in Eq. (2.5) has been replaced by $J(t)e^{-t/T_2}$]. The absorption spectrum shows a diffuse S_2 band with irregularly spaced structures, which cannot be assigned in terms of harmonic modes in the S_2 state.[4,64] The weak tail in the energy region of the S_1 state represents the well-known phenomenon of vibronic-intensity borrowing. It is seen that the semiclassical and the exact quantum results are in very good agreement in both parts of the spectrum.

It is interesting to compare this semiclassical result with a calculation Stock and Miller performed some time ago for the same model using a classical approach (i.e., without semiclassical phase information) based on the classical electron-analog model.[71] Although this classical method was able to reproduce the global features of the absorption spectrum, it was not capable of reproducing the finer structure. In contrast, the present semiclassical method describes these fine structures very well, demonstrating that the inclusion of phase information (and hence quantum interference) is important to describe the absorption spectrum in this system correctly.

B. 24-mode system-bath model

Within the four-mode model, the experimental absorption spectrum can only be obtained by including a rather

large phenomenological dephasing parameter $T_2=30$ fs. To account for this dephasing microscopically, Krempl *et al.* have extended the four-mode model by adding 20 weakly coupled tuning modes.[17,18] The Hamiltonian for this system-bath model is given by

$$\mathcal{H}_{\mathrm{SB}}=\mathcal{H}+\sum_{j=1}^{20}\frac{\omega_j}{2}(p_j^2+x_j^2)+\begin{pmatrix}\sum_{j=1}^{20}\kappa_j^{(1)}x_j & 0\\ 0 & \sum_{j=1}^{20}\kappa_j^{(2)}x_j\end{pmatrix}, \tag{3.2}$$

where $\mathcal{H}$ denotes the Hamiltonian of the four-mode model. The frequencies of the bath modes are equidistant in the interval [0.04 eV, 0.4 eV]. The coupling constants $\kappa_j^{(1)}=-\kappa_j^{(2)}$ were chosen at random in such a way that the overall coupling to the bath modes is weak compared to the coupling within the four-mode model (for the detailed parameters, see Ref. 17).

In pyrazine, 18 of the remaining 20 normal modes are nontotally symmetric and, therefore, can only couple quadratically to the electronic transition. Therefore, as Krempl *et al.* noted, this 24-mode system-bath model cannot represent pyrazine in a strict sense. Nevertheless, it is a good test example for relaxation in a strongly vibronically coupled system which in turn is weakly coupled to a harmonic bath. In particular, this model is ideally suited to study the performance of the semiclassical method for larger systems. It allows us to investigate the quality of the semiclassical approximation and the scaling of the numerical effort when the number of bath modes is increased gradually. To this end, we have performed two separate semiclassical calculations including 10 bath modes (the ones with the largest value of the coupling parameter κ_j/ω_j) and all 20 bath modes, respectively.

Let us first focus on the autocorrelation function. Figure 4 displays the modulus of the autocorrelation function for three different models: (a) without bath (the four-mode model from Sec. III A), (b) with 10 bath modes, and (c) with all 20 bath modes. The semiclassical results are compared with quantum results which have been obtained by Worth *et al.* using the MCTDH method.[74,75] The latter represents (within the accuracy relevant for the comparison with the semiclassical data) numerically exact results. It can be seen that the coupling to the bath leads to a strong suppression of the recurrences in the autocorrelation function. Although this damping becomes more pronounced when the number of bath modes is increased, the autocorrelation function retains a structure even with 20 bath modes included. Meyer, Cederbaum, and co-workers have shown[74,75] that this result is related to a selective damping of the high-energy states in the system-bath model considered.

The comparison between the semiclassical and the quantum results reveals a good overall agreement for the system-bath models in the short-time limit ($t<70$ fs). In particular, the damping of the first recurrence when the number of bath modes is increased is well reproduced by the semiclassical method. This is in contrast to more classical methods, such as the linearized semiclassical IVR/classical Wigner

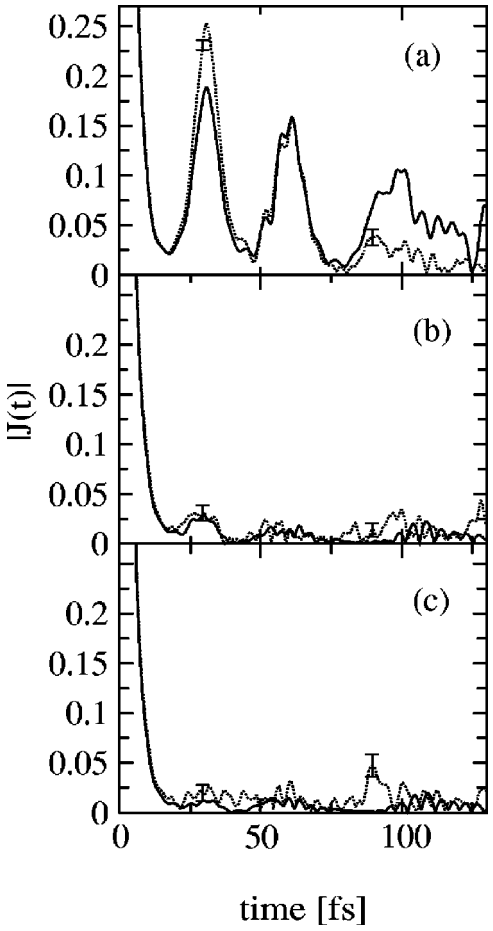

FIG. 4. Modulus of the autocorrelation function for the system-bath model. Shown are quantum (Ref. 74) (full line) and semiclassical (dotted line) results for a different number of modes: (a) four modes (without bath), (b) 14 modes (10 bath modes), and (c) 24 modes (20 bath modes). The error bars (for clarity, shown only at two times) represent the usual error estimate of the Monte Carlo integration.

method[107] which gives, for example, for the first recurrence in the 24-mode model an amplitude that is 1 order of magnitude too large.[108] As Müller and Stock have shown recently,[60,73,109] this failure to describe the correct relaxation behavior is related to an incorrect treatment of the zero-point energy in the classical implementation. The results in Fig. 4 demonstrate that the semiclassical method is capable of describing this effect correctly without requiring further zero-energy modifications. The rather large relative error at longer times, in particular for the 24-mode model, indicates a problem of the semiclassical calculation: As a result of the coupling to the bath, the autocorrelation function has a rather small amplitude (e.g., $|J(t)|<0.0025$ for $t>20$ fs in the 24-mode model). Such a small quantity is difficult to obtain with Monte Carlo integration schemes, in particular when the integrand is oscillatory, as is the case here.

The absorption spectra for the three different models are shown in Fig. 5. In contrast to the absorption spectrum for the four-mode model in Fig. 3, no phenomenological dephasing has been added (i.e., $1/T_2=0$). To reduce the effects of the finite propagation time ($t_{\max}=150$ fs) in the spectrum, the autocorrelation function is brought to zero smoothly at $t_{\max}$ by multiplying it by $\cos(\pi t/2t_{\max})$.[74] It is seen that the

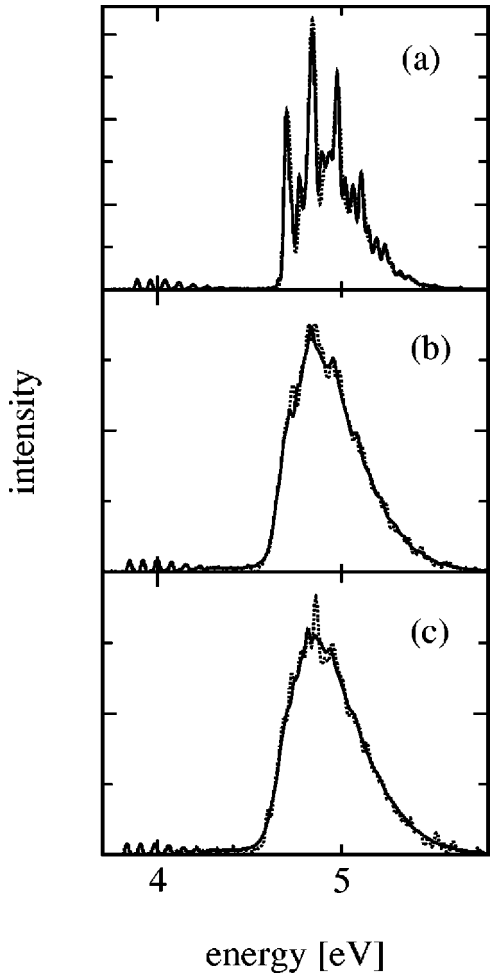

FIG. 5. Absorption spectra for the system-bath model. Shown are quantum (Ref. 74) (full line) and semiclassical (dotted line) results for a different number of modes: (a) four modes (without bath), (b) 14 modes (10 bath modes), and (c) 24 modes (20 bath modes).

coupling to the bath leads to a pronounced broadening of the spectrum in the S_2 band. In contrast, the vibrational peaks in the energy region of the S_1 state (which are due to vibronic-intensity borrowing, see above) are nearly unaffected by the coupling to the bath. It can also be seen that the region between the two bands obtains some intensity when the number of bath modes is increased. The comparison between the semiclassical and the quantum results shows that the semiclassical method can describe both parts of the spectrum rather well. The semiclassical result for the 24-mode model has more structure than the quantum result, which is presumably due to the rather high statistical error in the semiclassical calculation.

To conclude this section, we comment on the numerical effort of the calculation. The results in Fig. 4 panel (a) (four-mode model), panel (b) (14-mode model), and panel (c) (24-mode model) have been obtained by propagating $5\cdot10^6$, $15\cdot10^6$, and $7\cdot10^6$ trajectories, respectively. On a COMPAQ XP1000 workstation, the calculation for a fixed number of 10^6 trajectories takes approximately 15, 121, and 380 CPU hours, respectively, for the three different models. The comparison with the numerical effort of the MCTDH calculation of Worth *et al.* (see Ref. 74) shows that even though the total CPU time required for the semiclassical calculation is larger for all three models, the semiclassical method seems to have a slightly better scaling.[110] The required computer memory is of course much smaller in the semiclassical calculation (about 4 Mbyte for all three models).

C. 24-mode pyrazine model

The system-bath model considered in the previous section is able to describe the fast electronic dephasing process (which had to be included by hand for the four-mode model). As noted above, it cannot describe the true pyrazine molecule, because the additional 20 modes do not have the correct symmetry of the pyrazine molecule. This fact is reflected, for example, by the difference in the absorption spectra in Fig. 3 panel (b) and Fig. 5 panel (c). Recently, Raab *et al.* have presented MCTDH calculations based on a model Hamiltonian which takes into account the correct symmetry of all 24 normal modes of the pyrazine molecule.[76] In this model, the diabatic potential matrix is expanded up to second order around the equilibrium geometry of the electronic ground state

$$\mathbf{V}=\begin{pmatrix} E_1+\sum_{j\in G_1}\kappa_j^{(1)}x_j+\sum_{i,j\in G_2}\kappa_{i,j}^{(1)}x_ix_j & \lambda x_{10a}+\sum_{i,j\in G_4}\lambda_{i,j}^{(12)}x_ix_j \\ \lambda x_{10a}+\sum_{i,j\in G_4}\lambda_{i,j}^{(12)}x_ix_j & E_2+\sum_{j\in G_1}\kappa_j^{(2)}x_j+\sum_{i,j\in G_2}\kappa_{i,j}^{(2)}x_ix_j \end{pmatrix}. \tag{3.3}$$

Following the notation of Raab *et al.*, G_1 is the set of normal modes having A_g symmetry (within the D_{2h} point group). G_2 denotes the set of all pairs of modes with identical symmetry (e.g., $B_{2g}\times B_{2g}$). The set G_4 comprises all pairs of modes, the product of which has B_{1g} symmetry. The parameters of this Hamiltonian were determined by Raab *et al.* using *ab initio* calculations.[76] Compared to the system-bath Hamiltonian in Sec. III C, this model is considerably more complex, because all 24 modes of pyrazine enter both the diagonal and the off-diagonal part of the Hamiltonian. This higher complexity becomes manifest in an increased numerical effort both in the MCTDH[76] and the semiclassical calculation. In the latter case it results, for example, in a more chaotic classical dynamics, which in turn complicates the Monte Carlo integration.

Figure 6 displays the modulus of the autocorrelation

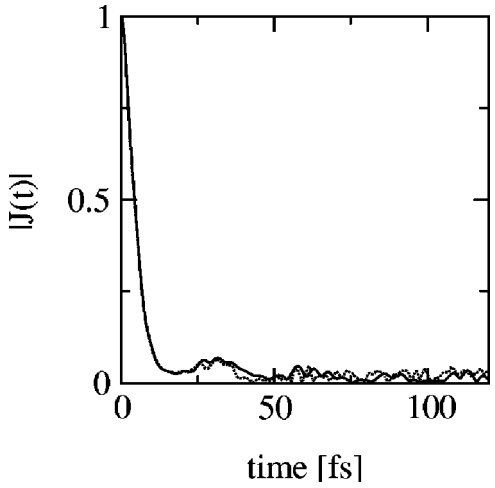

FIG. 6. Modulus of the autocorrelation function for the 24-mode pyrazine model. The full line is the quantum result (Ref. 76) and the dotted line is the semiclassical result.

function for the realistic 24-mode model. The semiclassical results are compared with the MCTDH results of Raab *et al.*[76] As for the 24-mode system-bath model in the previous section, the MCTDH results represent (within the accuracy required for the comparison with the semiclassical data) numerically exact results. The comparison with the four-mode model (Fig. 1) shows that the inclusion of the remaining 20 modes leads to a damping of the recurrences of the autocorrelation function. It is noted that this damping is not as strong as in the system-bath model [cf. Fig. 4, panel (c)]. The semiclassical result is seen to reproduce the quantum result rather well up to 70 fs; in fact, the agreement is better than in the case of the simpler system-bath model in Sec. III B.

Finally, Fig. 7 shows the absorption spectrum. As was done by Raab *et al.*, we have included a phenomenological broadening of $T_2=150$ fs to model the experimental broadening due to finite resolution and rotational motion. It can be seen that the inclusion of all 24 normal modes of the pyrazine molecule leads to a broadening of the spectrum which is in good agreement with the experimental result [Fig. 2, panel (b)]. In contrast to the system-bath model in Sec. III B, where the coupling to the bath results in a nearly structureless S_2 band, this structure is retained in the realistic 24-mode model. The semiclassical result is seen to be in fairly good agreement with the quantum result. As in the 24-mode system-bath model, the semiclassical spectrum has some spurious structure, which is presumably due to the rather high statistical error.

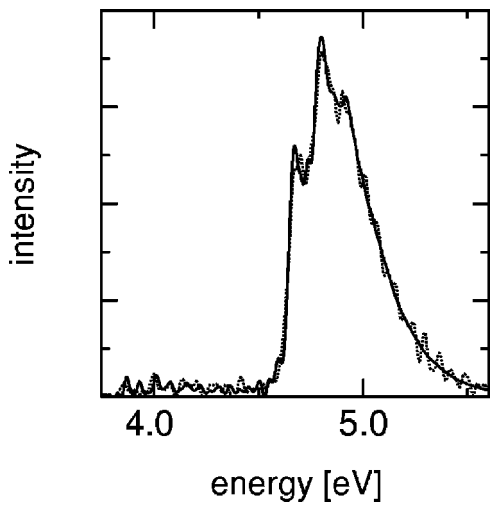

FIG. 7. Absorption spectrum for the 24-mode pyrazine model. The full line is the quantum result (Ref. 76) and the dotted line is the semiclassical result. In both spectra a phenomenological dephasing constant of $T_2=150$ fs was used.

IV. CONCLUSIONS

We have applied a recently proposed semiclassical approach to the nonadiabatic dynamics of the pyrazine molecule after photoexcitation to the S_2 electronic state. This system was chosen to test the new semiclassical method because it is one of the most extensively studied examples of vibronic coupling in polyatomic molecules. Furthermore, because the vibronic coupling in this system is rather strong, it is known to provide a stringent test for any approximate method.

The main purpose of the paper was to study the performance of the semiclassical method for larger systems. To this end, we have studied several vibronic coupling models for the S_1–S_2 conical intersection in pyrazine: a four-mode model including the four most strongly coupled modes, a system-bath model, which was obtained by coupling the four-mode model to an increasing number of bath modes, and, finally, a realistic 24-mode model. In all cases we have compared the semiclassical results with quantum results, which for the larger systems have been obtained by Meyer, Cederbaum, and co-workers[74–76] using the MCTDH method. The comparison demonstrates that the semiclassical approach is able to describe the ultrafast nonadiabatic dynamics in all of these models. In particular, we have found that the absorption spectrum and the autocorrelation function for shorter times ($t<80$ fs) is well reproduced by the semiclassical method.

Although this result is quite encouraging, it should be mentioned that the required numerical effort is rather large. We have found that, even though the required CPU time seems to have a slightly better scaling (with respect to the number of nuclear DoF) in the semiclassical approach than in the quantum MCTDH method, it is still larger in the 24-mode models. There are two main reasons for the rather large numerical effort in the semiclassical calculation: (i) Although we have used an integral conditioning (smoothing) technique, the oscillatory nature of the integrand still requires a large number of trajectories to converge the Monte Carlo integration. (ii) Due to the calculation of the preexponential factor, the numerical effort per trajectory has an unfavorable $(2+N)^3$ scaling (with N being the number of nuclear DoF). Both problems need to be addressed further to make the semiclassical approach practical for larger systems.

In the present work, we have focused on the calculation of the autocorrelation function and the absorption spectrum. Another important quantity to characterize the dynamics in vibronically coupled systems is the population of the diabatic

(or adiabatic) electronic states. Although the semiclassical approach outlined in this paper is in principle capable of describing this quantity (see, for example, Refs. 55, 56 and 59), it becomes practically unfeasible in larger systems because one either has to store the semiclassical wave function in full dimensionality or to use a double phase space formulation. In this respect, the forward–backward IVR methods proposed recently[87,111–114] appear to be a promising alternative. Work in this direction is in progress.

ACKNOWLEDGMENTS

We would like to thank N. T. Maitra and H. Wang for several helpful discussions throughout this project. Furthermore, we thank A. Raab, G. A. Worth, H.-D. Meyer, and L. S. Cederbaum for providing their quantum-mechanical results. This work was supported by the Director, Office of Science, Office of Basic Energy Sciences, Chemical Sciences Division of the U. S. Department of Energy under Contract No. DE-AC03-76SF00098, and by National Science Foundation Grant No. CHE 97-32758. M.T. gratefully acknowledges a Feodor–Lynen fellowship of the Alexander von Humboldt Foundation.

[1] H. Köppel, W. Domcke, and L. S. Cederbaum, Adv. Chem. Phys. **57**, 59 (1984).
[2] J. Michl and V. Bonačić-Koutecký, *Electronic Aspects of Organic Photochemistry* (Wiley, New York, 1990).
[3] M. Klessinger and J. Michl, *Excited States and Photochemistry of Organic Molecules* (VCH, New York, 1995).
[4] W. Domcke and G. Stock, Adv. Chem. Phys. **100**, 1 (1997).
[5] E. J. Heller, J. Chem. Phys. **64**, 63 (1976).
[6] R. B. Gerber, V. Buch, and M. A. Ratner, J. Chem. Phys. **77**, 3022 (1982).
[7] S. Sawada and H. Metiu, J. Chem. Phys. **84**, 227 (1986).
[8] Z. Kotler, E. Neria, and A. Nitzan, Comput. Phys. Commun. **63**, 234 (1991).
[9] H.-D. Meyer, U. Manthe, and L. S. Cederbaum, Chem. Phys. Lett. **165**, 73 (1990).
[10] U. Manthe, H.-D. Meyer, and L. S. Cederbaum, J. Chem. Phys. **97**, 3199 (1992).
[11] M. H. Beck, A. Jäckle, G. A. Worth, and H.-D. Meyer, Phys. Rep. **324**, 1 (2000).
[12] C. H. Mak and D. Chandler, Phys. Rev. A **44**, 2352 (1991).
[13] R. Egger and C. H. Mak, Phys. Rev. B **50**, 15210 (1994).
[14] D. E. Makarov and N. Makri, Phys. Rev. A **48**, 3626 (1993).
[15] N. Makri and D. E. Makarov, Chem. Phys. Lett. **221**, 482 (1994).
[16] M. Winterstetter and W. Domcke, Phys. Rev. A **47**, 2838 (1993).
[17] S. Krempl, M. Winterstetter, H. Plöhn, and W. Domcke, J. Chem. Phys. **100**, 926 (1994).
[18] S. Krempl, M. Winterstetter, and W. Domcke, J. Chem. Phys. **102**, 6499 (1995).
[19] V. May and M. Schreiber, Chem. Phys. Lett. **181**, 267 (1991).
[20] O. Kühn, V. May, and M. Schreiber, J. Chem. Phys. **101**, 10404 (1994).
[21] Y. Tanimura and S. Mukamel, J. Chem. Phys. **101**, 3049 (1994).
[22] W. T. Pollard and R. A. Friesner, J. Chem. Phys. **100**, 5054 (1994).
[23] J. M. Jean and G. R. Fleming, J. Chem. Phys. **103**, 2092 (1995).
[24] B. Wolfseder and W. Domcke, Chem. Phys. Lett. **235**, 370 (1995).
[25] B. Wolfseder, L. Seidner, G. Stock, W. Domcke, M. Seel, S. Engleitner, and W. Zinth, Chem. Phys. **233**, 323 (1998).
[26] N. F. Mott, Proc. Cambridge Philos. Soc. **27**, 553 (1931).
[27] J. B. Delos and W. R. Thorson, Phys. Rev. A **6**, 720 (1972).
[28] G. D. Billing, Chem. Phys. Lett. **30**, 391 (1975).
[29] D. A. Micha, J. Chem. Phys. **78**, 7138 (1983).
[30] R. Graham and M. Höhnerbach, Z. Phys. B: Condens. Matter **57**, 233 (1984).
[31] G. D. Billing, J. Chem. Phys. **99**, 5849 (1993).
[32] G. Stock, J. Chem. Phys. **103**, 2888 (1995).
[33] J. C. Tully and R. K. Preston, J. Chem. Phys. **55**, 562 (1971).
[34] W. H. Miller and T. F. George, J. Chem. Phys. **56**, 5637 (1972).
[35] J. C. Tully, J. Chem. Phys. **93**, 1061 (1990).
[36] M. F. Herman, J. Chem. Phys. **76**, 2949 (1982).
[37] F. J. Webster, P. J. Rossky, and R. A. Friesner, Comput. Phys. Commun. **63**, 494 (1991).
[38] S. Chapman, Adv. Chem. Phys. **82**, 423 (1992).
[39] D. F. Coker and L. Xiao, J. Chem. Phys. **102**, 496 (1995).
[40] P. Jungwirth and R. B. Gerber, J. Chem. Phys. **102**, 6046 (1995).
[41] T. J. Martinez, M. Ben-Nun, and R. D. Levine, J. Phys. Chem. **100**, 7884 (1996).
[42] A. Ferretti, A. Lami, and G. Villani, J. Chem. Phys. **106**, 934 (1997).
[43] C. C. Martens and J.-Y. Fang, J. Chem. Phys. **106**, 4918 (1997).
[44] R. Kapral and G. Ciccotti, J. Chem. Phys. **110**, 8919 (1999).
[45] See, e.g., the discussion in P. J. Kuntz, J. Chem. Phys. **95**, 141 (1991).
[46] P. Pechukas, Phys. Rev. **181**, 174 (1969).
[47] M. C. Gutzwiller, *Chaos in Classical and Quantum Mechanics* (Springer, New York, 1990).
[48] F. J. Webster, E. T. Wang, P. J. Rossky, and R. A. Friesner, J. Chem. Phys. **100**, 4835 (1994).
[49] W. H. Miller and C. W. McCurdy, J. Chem. Phys. **69**, 5163 (1978).
[50] C. W. McCurdy, H.-D. Meyer, and W. H. Miller, J. Chem. Phys. **70**, 3177 (1979).
[51] H.-D. Meyer and W. H. Miller, J. Chem. Phys. **70**, 3214 (1979).
[52] H.-D. Meyer and W. H. Miller, J. Chem. Phys. **71**, 2156 (1979).
[53] L. M. Raff and D. L. Thompson, in *Theory of Chemical Reaction Dynamics*, edited by M. Baer (CRC, Boca Raton, FL, 1985), Vol. 3.
[54] W. H. Miller, Adv. Chem. Phys. **25**, 69 (1974).
[55] G. Stock and M. Thoss, Phys. Rev. Lett. **78**, 578 (1997).
[56] M. Thoss and G. Stock, Phys. Rev. A **59**, 64 (1999).
[57] J. Schwinger, in *Quantum Theory of Angular Momentum*, edited by L. C. Biedenharn and H. V. Dam (Academic, New York, 1965).
[58] J. R. Klauder, Phys. Rev. D **19**, 2349 (1979).
[59] X. Sun and W. H. Miller, J. Chem. Phys. **106**, 916 (1997).
[60] U. Müller and G. Stock, J. Chem. Phys. **108**, 7516 (1998).
[61] F. Grossmann, Phys. Rev. A **60**, 1791 (1999).
[62] V. S. Batista and W. H. Miller, J. Chem. Phys. **108**, 498 (1998).
[63] E. Coronado, V. S. Batista, and W. H. Miller, J. Chem. Phys. **112**, 5566 (2000).
[64] R. Schneider, W. Domcke, and H. Köppel, J. Chem. Phys. **92**, 1045 (1990).
[65] G. Stock, R. Schneider, and W. Domcke, J. Chem. Phys. **90**, 7184 (1989).
[66] G. Stock and W. Domcke, J. Chem. Phys. **93**, 5496 (1990).
[67] L. Seidner, G. Stock, A. L. Sobolewski, and W. Domcke, J. Chem. Phys. **96**, 5298 (1992).
[68] A. L. Sobolewski, C. Woywod, and W. Domcke, J. Chem. Phys. **98**, 5627 (1993).
[69] C. Woywod, W. Domcke, A. L. Sobolewski, and H.-J. Werner, J. Chem. Phys. **100**, 1400 (1994).
[70] G. Stock, C. Woywod, W. Domcke, T. Swinney, and B. S. Hudson, J. Chem. Phys. **103**, 6851 (1995).
[71] G. Stock and W. H. Miller, Chem. Phys. Lett. **197**, 396 (1992).
[72] U. Müller and G. Stock, J. Chem. Phys. **107**, 6230 (1997).
[73] U. Müller and G. Stock, J. Chem. Phys. **111**, 77 (1999).
[74] G. A. Worth, H.-D. Meyer, and L. S. Cederbaum, J. Chem. Phys. **109**, 3518 (1998).
[75] G. A. Worth, H.-D. Meyer, and L. S. Cederbaum, Chem. Phys. Lett. **299**, 451 (1999).
[76] A. Raab, G. A. Worth, H.-D. Meyer, and L. S. Cederbaum, J. Chem. Phys. **110**, 936 (1999).
[77] F. Dushinsky, Acta Physicochim. URSS **77**, 551 (1936).
[78] For a calculation of the S_2-absorption spectrum of pyrazine including temperature effects see, for example, A. Raab, I. Burghardt, and H.-D. Meyer, J. Chem. Phys. **111**, 8759 (1999).
[79] E. J. Heller, J. Chem. Phys. **75**, 2923 (1981).
[80] M. F. Herman and E. Kluk, Chem. Phys. **91**, 27 (1984).
[81] E. J. Heller, J. Chem. Phys. **94**, 2723 (1991).
[82] K. G. Kay, J. Chem. Phys. **100**, 4377 (1994).
[83] A. R. Walton and D. E. Manolopoulos, Mol. Phys. **87**, 961 (1996).
[84] M. Ovchinnikov and V. A. Apkarian, J. Chem. Phys. **108**, 2277 (1998).
[85] W. H. Miller, J. Chem. Phys. **53**, 3578 (1970).
[86] M. A. Sepulveda and F. Grossmann, Adv. Chem. Phys. **96**, 191 (1996).
[87] W. H. Miller, Faraday Discuss. **110**, 1 (1998).
[88] F. Grossmann, Comments At. Mol. Phys. **34**, 243 (1999).
[89] K. G. Kay, J. Chem. Phys. **101**, 2250 (1994).
[90] B. W. Spath and W. H. Miller, J. Chem. Phys. **104**, 95 (1996).

[91] M. F. Herman, Chem. Phys. Lett. **275**, 445 (1997).
[92] B. E. Guerin and M. F. Herman, Chem. Phys. Lett. **286**, 361 (1998).
[93] Y. Elran and K. G. Kay, J. Chem. Phys. **110**, 8912 (1999).
[94] V. S. Filinov, Nucl. Phys. B **271**, 717 (1987).
[95] N. Makri and W. H. Miller, Chem. Phys. Lett. **139**, 10 (1987).
[96] J. D. Doll, D. L. Freeman, and T. L. Beck, Adv. Chem. Phys. **78**, 61 (1994).
[97] H.-K. Hong and C. W. Jakobson, J. Chem. Phys. **68**, 1170 (1978).
[98] I. Suzaka, Y. Udagawa, and M. Ito, Chem. Phys. Lett. **64**, 333 (1979).
[99] Y. Udagawa, M. Ito, and I. Suzaka, Chem. Phys. **46**, 237 (1980).
[100] D. B. McDonald and S. A. Rice, J. Chem. Phys. **74**, 4893 (1981).
[101] J. Kommandeur, W. A. Majewski, W. L. Meerts, and D. W. Pratt, Annu. Rev. Phys. Chem. **38**, 433 (1987).
[102] A. Amirav, Chem. Phys. **126**, 327 (1988).
[103] K. K. Innes, I. G. Ross, and W. R. Moomaw, J. Mol. Spectrosc. **132**, 492 (1988).
[104] For a discussion of the nonunitarity of the semiclassical approximation in the context of nonadiabatic dynamics see, for example, Ref. 56.
[105] N. T. Maitra, J. Chem. Phys. **112**, 531 (2000).
[106] I. Yamazaki, T. Murao, T. Yamanaka, and K. Yoshihara, Faraday Discuss. **75**, 395 (1983).
[107] X. Sun, H. Wang, and W. H. Miller, J. Chem. Phys. **109**, 7064 (1998).
[108] M. Thoss and W. H. Miller (unpublished).
[109] G. Stock and U. Müller, J. Chem. Phys. **111**, 65 (1999).
[110] For a discussion of the scaling of semiclassical IVR methods in the context of the calculation of Franck–Condon spectra, see, for example, M. L. Brewer, J. S. Hulme, and D. E. Manolopoulos, J. Chem. Phys. **106**, 4832 (1997); M. L. Brewer, *ibid.* **111**, 6168 (1999).
[111] N. Makri and K. Thompson, Chem. Phys. Lett. **291**, 101 (1998).
[112] X. Sun and W. H. Miller, J. Chem. Phys. **110**, 6635 (1999).
[113] K. Thompson and N. Makri, Phys. Rev. E **59**, 4729 (1999).
[114] H. Wang, M. Thoss, and W. H. Miller, J. Chem. Phys. **112**, 47 (2000).